SUPPLEMENTARY INFORMATION

Experimental Clocking of Nanomagnets with Strain for Ultra Low Power Boolean Logic

Noel D'Souza[a], Mohammad Salehi Fashami[a], Supriyo Bandyopadhyay[b] and Jayasimha Atulasimha[a,*]

[a]Dept. of Mechanical and Nuclear Engineering

[b]Dept. of Electrical and Computer Engineering,

Virginia Commonwealth University, Richmond, VA 23284, USA.

*Email: jatulasimha@vcu.edu

In the main paper, we demonstrated strain-clocked switching of magnetostrictive Co nanomagnets fabricated on a bulk PMN-PT piezoelectric substrate. Owing to the shape anisotropy, the elliptical Co nanomagnets have two stable states for magnetization orientation – 'up' (↑) and 'down' (↓) – along the major axis. Magnetization rotation is accomplished via the Villari effect, or the inverse magnetostrictive effect, in which a strain/stress induces a magnetization rotation in the Co nanomagnets. This strain is produced when a voltage is applied between two electrodes delineated on the PMN-PT substrate. The substrate deforms, generating a strain that is transferred to the magnetostrictive Co layer, which is in elastic contact with the substrate. In this supplement, we present the characterization of the strain developed in the PMN-PT substrate as a function of the applied voltage and the calculation of stress and shape anisotropies in nanomagnets of various nominal dimensions, as well as the sensitivity of these anisotropies to variations in the nanomagnet dimensions. We further present additional experimental data on switching behavior for the following cases: (i) Isolated magnet, (ii) Dipole-coupled pair, and (iii) Dipole-coupled chain of nanomagnets. Finally, we provide scaling and

energy calculations to demonstrate the potential of this paradigm in achieving ultra-low power Boolean computing.

Supplementary Section A: Experimental Setup and Anisotropy Energy Calculations

A.1 Experimental Methods

A bulk (001) PMN-PT 70/30 substrate of dimensions (5×5×0.5) mm^3 was initially poled along the length with an electric field of 800 kV m^{-1} in a castor oil bath. Subsequently, the substrate was cleaned in acetone and IPA and a bilayer of positive e-beam resist (495K PMMA and 950K PMMA; 2% Anisole) was spin-coated as follows:

A static dispense of ~3 ml (495K PMMA) was carried out on the PMN-PT substrate followed by a dynamic spread at 500 rpm for 5 seconds. The spin cycle was performed at a rate of 4000 rpm for 45 seconds. A pre-bake at 115 °C (so as not to exceed the PMN-PT Curie temperature of 150 °C) was then performed for 90 seconds, resulting in a 495K PMMA layer of ~50 nm. The top 950K PMMA layer was spin-coated next using the same procedure.

Electron-beam lithography was performed at 30 kV using a Hitachi SU-70 SEM in conjunction with the Nabity NPGS nanolithography system. A beam current of 60 pA and dose of 150 – 250 μC cm^{-2} was used to create the elliptical structures. The PMMA-coated substrate is then developed in an MIBK:IPA (1:3) [(methyl isobutyl ketone: isopropyl alcohol)] solution for 70 seconds, rinsed in IPA for 20 seconds to remove the exposed PMMA and finally blow-dried.

A 12 nm layer of Co (above a 5 nm Ti adhesion layer deposited at 0.5 angstrom/s) was then deposited at 0.3 angstrom/s using an electron-beam evaporator at a base pressure of ~3.5×10^{-7}

Torr. Finally, lift-off was performed by soaking the substrate in acetone for ~5 minutes at 30 °C and using an ultrasonic cleaner for 10 seconds to strip off the Ti/Co layers above the unexposed PMMA regions. Magnetic characterization of the elliptical nanomagnets is performed using a Veeco Atomic Force Microscope (AFM) with low-moment magnetic force microscope tips (Bruker MESP-LM) at a lift height of 60 nm.

A.2 Experimental characterization of strain generated in the PMN-PT substrate

The piezoelectric substrate used in our experiments was a polished (001)-oriented (1-x)[$Pb(Mg_{1/3}Nb_{2/3})O_3$]–x[$PbTiO_3$] (PMN-PT) substrate (where x = 0.3) of dimensions 5×5×0.5 mm^3 supplied by Atom Optics Co Ltd. In order to measure the strain response of the PMN-PT substrate, we attach a general purpose 120 Ω Constantan linear foil strain gauge (EA-06-062ED-120) Vishay Precision Group, Micro-Measurements) to the top surface of the PMN-PT substrate and measure the strain using a P3 Strain Recorder and Indicator (Vishay Precision Group). Electrodes are attached to the edges of the substrate using silver paste and a voltage is applied along the length of the substrate using a Xantrex XFR20-60 DC power supply in conjunction with a Trek 10/10B high voltage amplifier. Poling is performed in a castor oil bath to prevent arcing at high voltages. An electric field of 800 kV/m is applied along the length of the substrate at a rate of ~1 kV/min. The strain response of the PMN-PT is then measured using the P3 strain recorder, as shown in the strain-voltage curves of Figure S1. Following PMN-PT poling along the length of the substrate (the direction of P in the inset illustrates the direction of polarization), the strain response is determined for various voltages. It can be seen that for a voltage of 1.5 kV (E = 300 kV/m), a strain of ~300 ppm is observed, while at V = 2 kV (E = 400 kV/m), a strain of

~400 ppm can be generated. For our numerical calculations, we use the following material constants for a) Co: Young's modulus, Y = 209 GPa[1], saturation magnetization, M_s = 14.22 × 10^5 A/m [2], magnetostrictive constant, $(^3/_2 \lambda_s)$ = -5 × 10^{-5} [2,3]; and b) PMN-PT: Young's modulus, Y ~20–80 GPa [4,5] (since the PMN-PT is 500 microns thick and the Co is 12 nm thick, the PMN-PT is much stiffer than the Co and most of the strain in the PMN-PT is transferred to the Co independent of the actual value of the Young's Modulus of the PMN-PT layer), Curie temperature, T_c = 150 °C [5]. The d_{33} value of (001) PMN-PT experimentally measured in our experiments (~1000 pm/V) is in agreement with other experimentally derived d_{33} values[5–8].

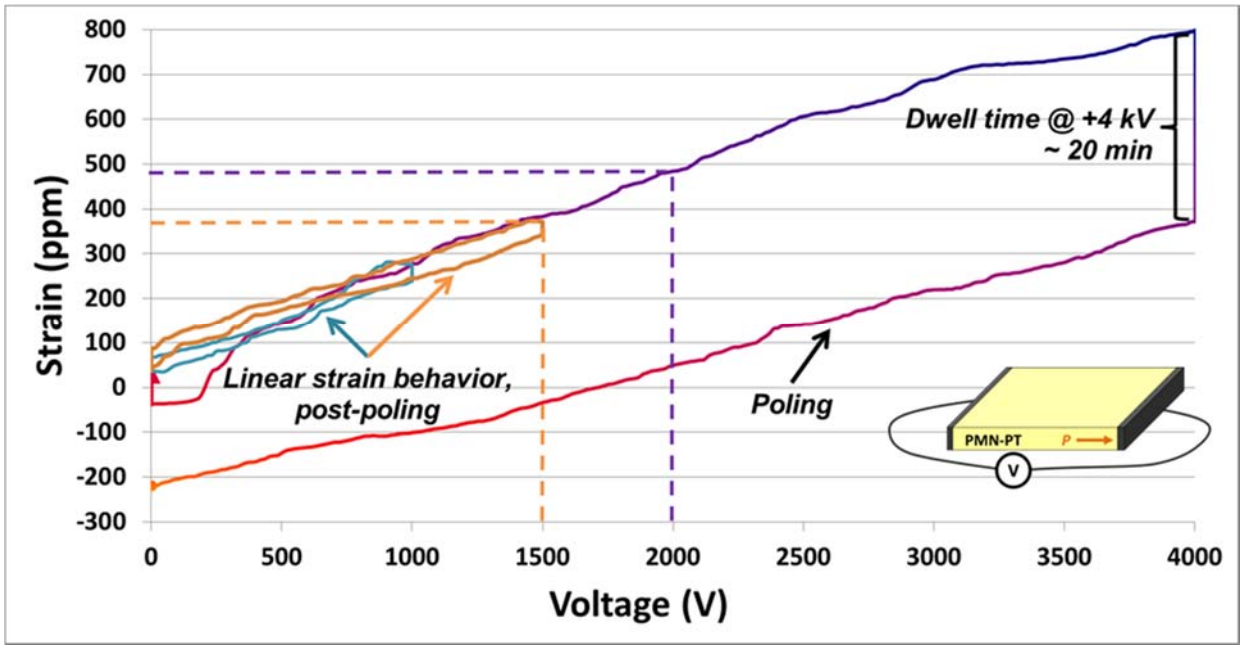

Figure S1: Strain response curves for bulk (001) PMN-PT substrate of dimensions 5×5×0.5 mm³. Poling of the substrate is performed in a castor oil bath with an electric field of 800 kV/m (V = 4 kV). Measurement of the strain response of the poled substrate is then carried out for various fields. A linear strain response can be observed, with a strain of ~300 ppm generated for V = 1.5 kV and ~400 ppm for V = 2 kV.

Thus, if a strain of ~400 ppm is transferred to the Co layer, it corresponds to a stress $\sigma = Y \times$ strain ~80 MPa developed in it. [*Note: In addition to the d_{33} induced strain along the direction of the applied field, there is an additional d_{31} induced strain. However, since the Poisson's ratios of both Co and PMN-PT are ~0.3, although the strain experienced in the in-plane perpendicular direction of the Co nanomagnet is non-zero, the matched strain in both materials results in negligible stress experienced along this direction. Therefore, it can be assumed that a predominantly uniaxial tensile stress is applied along the direction of the applied field*]. Also, Co nanomagnets are fabricated, as described in the Methods Summary section at the end of this Supplement, on another similarly-poled PMN-PT substrate of the same dimensions (and not on the substrate used in the strain measurements).

The nanomagnet dimensions are chosen according to the criteria as mentioned in the main paper. Lithographic and dosage variations make the lateral dimensions of a nanomagnet differ from the nominal values. Deposition rate variation during evaporation of the metals (magnets) makes the thickness random. Another source of variability that is seldom appreciated is oxidation of the Co layer due to repeated handling under atmospheric conditions that reduces the effective dimensions of the nanomagnet (lateral and thickness). In the case of the nanomagnet of nominal dimensions (250×150×12) nm^3, a ~5% variation in dimensions (lateral and thickness) will result in lower and upper bound dimensions of (237×157×11) nm^3 and (263×142×13) nm^3, respectively. Similarly, the lower and upper bounds of the second nanomagnet's dimensions are (190×183×11) nm^3 and (210×167×13) nm^3, respectively. Finally, the same bounds for the third nanomagnet are (190×194×11) nm^3 and (210×176×13) nm^3, respectively. It can be seen that for the nanomagnet with weakest shape anisotropy (third), a 5% variation in dimensions results in a

'lower bound' nanomagnet with the easy (long) axis along the horizontal, rather than the vertical, axis!

A.3 Estimation of the stress anisotropy energy in the Co nanomagnet dots

Next, we calculate the anisotropy energies of the Co nanomagnets having nominal dimensions of (250×150×12) nm^3, (200×175×12) nm^3 and (200×185×12) nm^3.

The stress anisotropy energy of a nanomagnet can be expressed as[9]:

$$E_{stress-anisotropy} = \left(-\tfrac{3}{2}\lambda_s\right)\sigma\Omega, \quad (1)$$

where ($\tfrac{3}{2}\lambda_s$) is the saturation magnetostriction of Co, σ is the stress applied to the nanomagnet and Ω is its volume. A tensile stress is taken to be positive while a compressive stress is negative. Therefore, the stress anisotropy energies of the Co nanomagnets having nominal dimensions as stated above are 8.8 eV, 8.2 eV and 8.7 eV, respectively, for a stress of ~80 MPa in the Co layer.

The stress anisotropy energies associated with the Co nanomagnets of nominal dimensions, as well as with a 5% variation, are displayed in Table S1.

Table S1. Stress anisotropy energy of Co nanomagnets

Nominal Dimensions	**Stress Anisotropy Energy (eV) for Nominal dimensions**	**Stress Anisotropy Energy (eV) w/ ±5% variation in dimensions**
250×150×12 nm^3 (high shape anisotropy)	**~ 8.8**	**(8 – 9.5)**

200×175×12 nm^3 (low shape anisotropy)	**~ 8.2**	**(7.5 – 9)**
200×185×12 nm^3 (lowest shape anisotropy)	**~ 8.7**	**(8 – 9.4)**

A.4 Estimation of the shape anisotropy energy in the Co nanomagnets

Next, we calculate the shape anisotropy energy of the nanomagnets which is given by[9]:

$$E_{shape-anisotropy} = \left(\frac{\mu_0}{2}\right)\left[M_s^2 \Omega\right] N_d \tag{2}$$

where μ_0 is the permeability of free space, M_s is the saturation magnetization of Co and N_d is the demagnetization factor. We consider the Co nanomagnet to be a very flat ellipsoid[10] with the diameters of the major and minor axis as a and b, and with a thickness c (for $a \geq b >> c$). The expressions for N_d along the major (long) axis and minor (short) axis are[10]:

$$N_{d\_xx} = \frac{c}{a}(1-e^2)\frac{K-E}{e^2}, \quad N_{d\_yy} = \frac{c}{a}\frac{E-(1-e^2)K}{e^2(1-e^2)^{\frac{1}{2}}}, \tag{3}$$

where K and E are complete elliptical integrals[11] with argument $e = (1-b^2/a^2)^{\frac{1}{2}}$

The shape anisotropy energies associated with the Co nanomagnets of nominal dimensions, as well as with a 5% variation, are displayed in Table S2. As can be seen, the shape anisotropy energy of the nanomagnet having the lowest shape anisotropy is still high enough that it would not be affected by random thermal noise at room temperature, thereby minimizing static error

probability. However, small variations in dimensions can tip the balance in favor of high shape anisotropy (larger than stress anisotropy energy + dipole energy in case of pairs or coupled arrays) so there would not be many nanomagnets that can switch. Of course, in addition to dimensional variations, pinning sites and defects would also affect the effective barrier for switching.

Table S2. Shape anisotropy energy of Co nanomagnets

Nominal Dimensions	**Shape Anisotropy Energy (eV) for Nominal dimensions**	**Shape Anisotropy Energy (eV) w/ ±5% variation in dimensions**
250×150×12 nm^3 (high shape anisotropy)	**~ 105**	**(71 – 148)**
200×175×12 nm^3 (low shape anisotropy)	**~ 26**	**(6 – 53)**
200×185×12 nm^3 (lowest shape anisotropy)	**~ 16**	**(4 – 42)**

One could argue that designing the second and third nanomagnets with even lower shape anisotropy would have ensured that the stress anisotropy would rotate a greater number of nanomagnets. However, consider the third nanomagnet with lowest shape anisotropy having nominal dimensions of (200×185×12) nm^3. A 5% variation in every dimension could result in a nanomagnet of dimensions ~ (190×194×11) nm^3. It is easy to see that such a nanomagnet would have its easy (long) axis along the horizontal, rather than the vertical, axis, and inhibit propagation of information along the nanomagnet array. Therefore, while nanomagnets with nominal dimensions of, say, (200×190×8) nm^3 and (200×195×8) nm^3 would have shape

anisotropy energies of ~4.7 eV and ~2.3 eV, respectively, and stress anisotropy energies of ~6 eV and ~6.1 eV (generated by 80 MPa stress) will be enough to rotate the magnetization, the possibility of finding nanomagnets with incorrect easy axes (along the horizontal instead of vertical) will also be greater. Furthermore, note that the lower the shape anisotropy, the higher the possibility of tip-induced effects from the MFM tip, which may cause magnetization reorientation during scanning.

Considering the complexities described above, one can appreciate the tight fabrication tolerance of this scheme, especially when considering an array of multiple nanomagnets with decreasing shape anisotropies. Failure to satisfy this strict tolerance accounts for the low percentage of nanomagnets that switch correctly, as shown in the MFM results of Section C of this Supplement. We also point out that such strict lithographic tolerances may be daunting for an academic lab, but is par for the course in an industrial foundry.

Supplementary Section B: Nanomagnet and Substrate Characterization

a. Nanomagnet characterization

Figure S2 displays several SEM micrographs to show the quality of the fabricated Co nanomagnets on a PMN-PT substrate. In addition, AFM topography images (Figure S3) illustrate the quality of the nanomagnets (roughness, thickness and lateral dimensions).

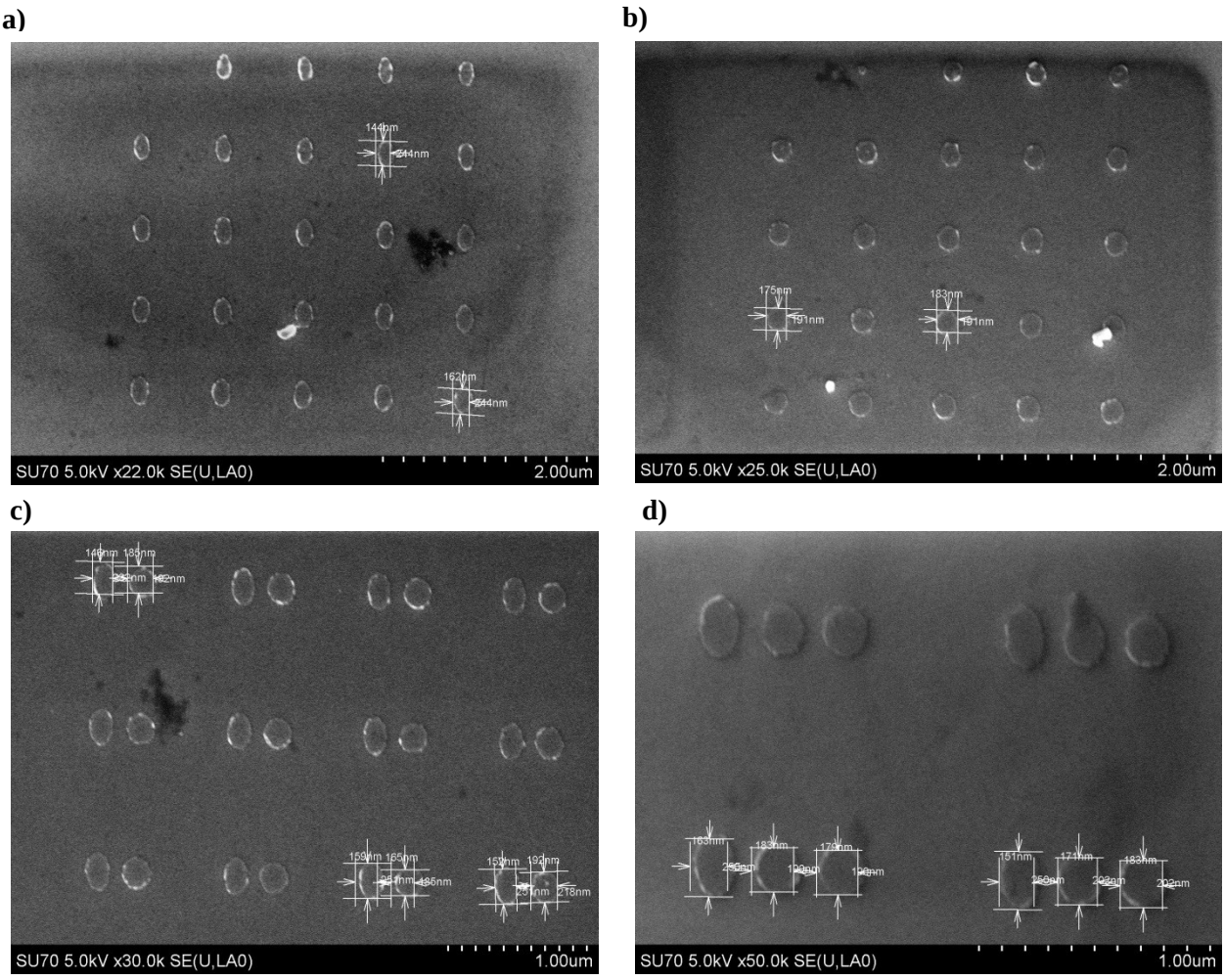

Figure S2. Co nanomagnets fabricated on PMN-PT substrate. The following scenarios are considered, having the corresponding lateral dimensions: a) Isolated, (250 nm x 150 nm), b) Isolated, (200 nm x 185 nm), c) Dipole-coupled with inter-magnet spacing of 315 nm, (250 nm x 150 nm, 200 nm x 185 nm), d) Array with inter-magnet spacing of 315 nm, (250 nm x 150 nm, 200 nm x 175 nm x 185 nm). Thickness = 16.5 nm (5 nm Ti + 11.5 nm Co).

In Figure S3, the height of one particular nanomagnet is measured to be ~ 15.3 nm. The nominal height of the fabricated nanomagnets is 16.5 nm (5 nm Ti + 11.5 nm Co).

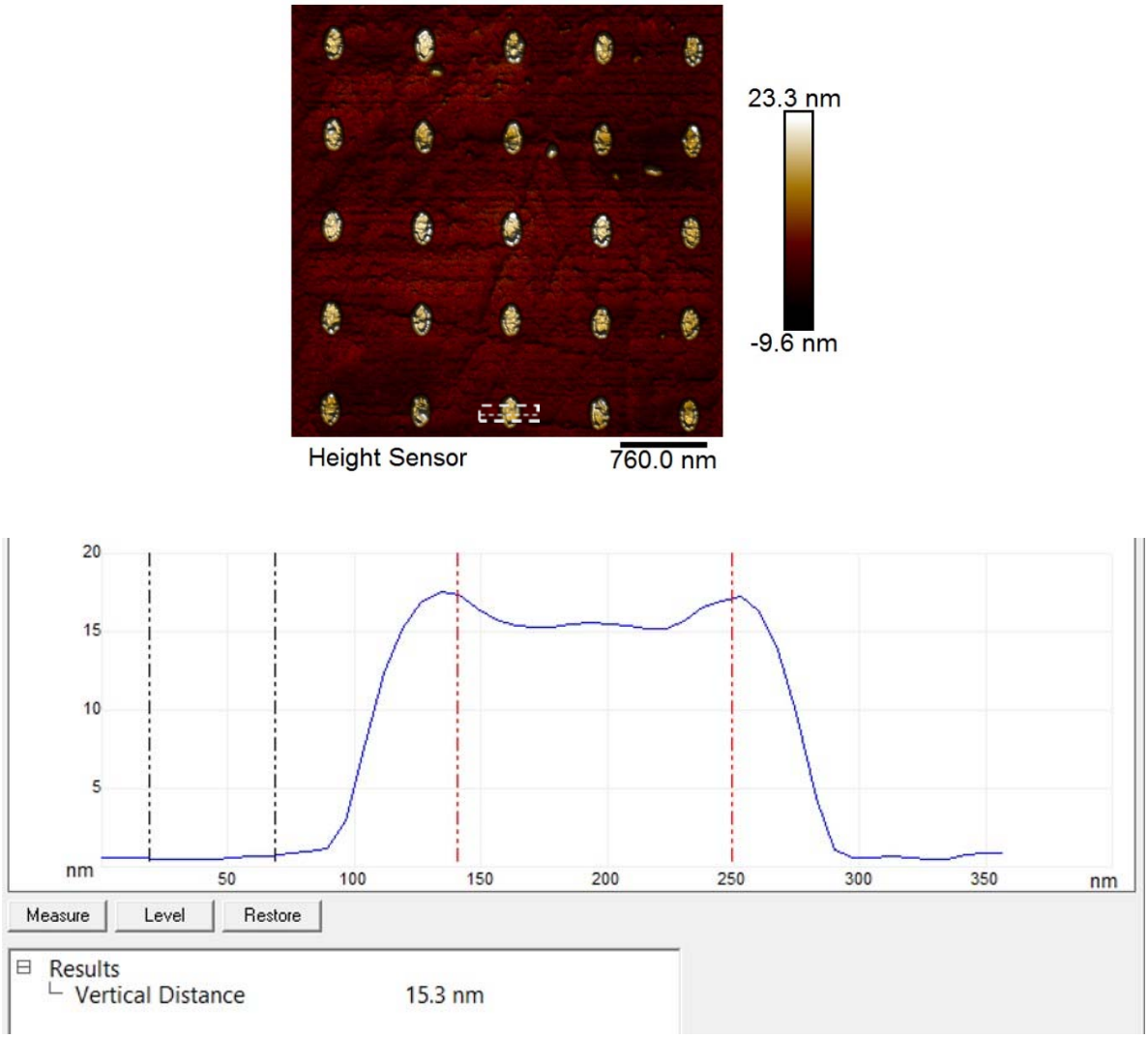

Figure S3. Height measurement of Co nanomagnet on PMN-PT substrate. (Note: Total thickness of magnet = 5 nm Ti + 11.5 nm Co).

b. PMN-PT surface roughness characterization

The surface roughness of the substrate is ~1.7 – 2 nm. As shown in Figure S4, a 15 μm x 15 μm region of the PMN-PT substrate shows R_q (root mean square roughness) and R_a (average

roughness) values of the particular scanned region. A smaller 7.2 μm x 7.2 μm section was also studied since this corresponds to the largest area of our nanomagnet arrays (array of 3 magnets). Local variations in the roughness can rise up to ~3 nm. These surface incongruities are taken into account for potential peculiar switching mechanisms in our MFM studies as such occurrences, though very rare, lead to unclear magnetic states and were discarded from our switching results/claims of correct switching.

a)

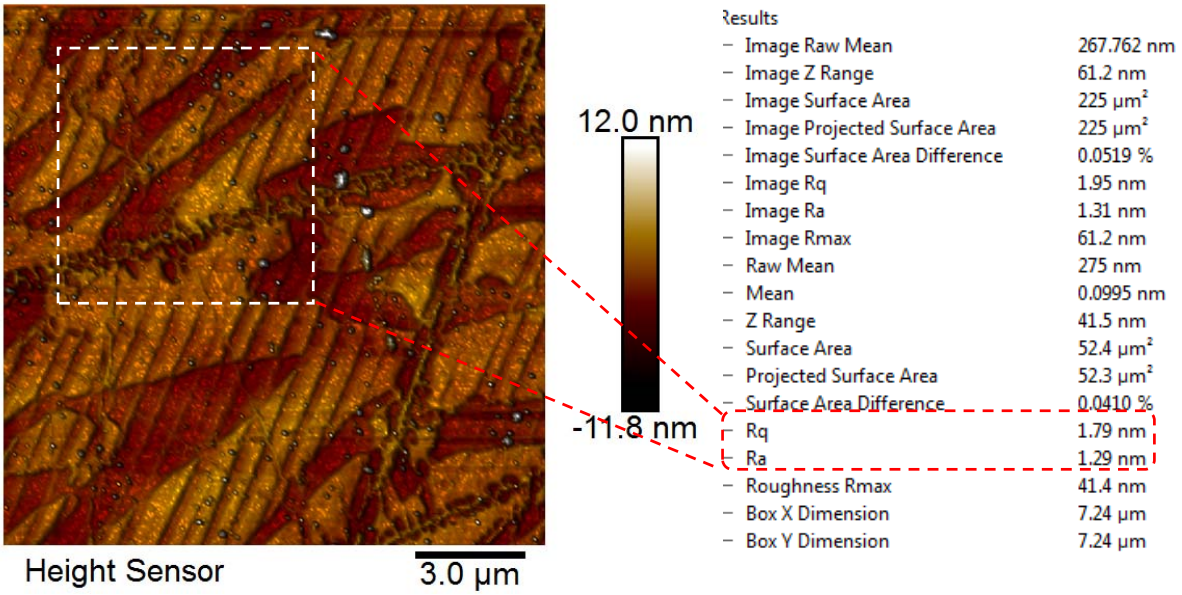

b)

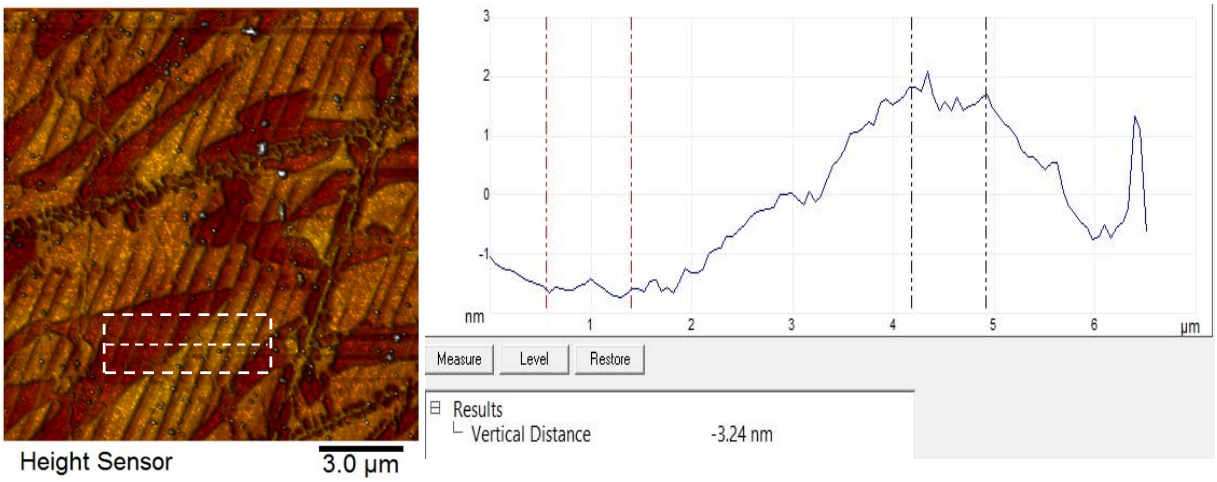

Figure S4. a) Surface roughness of PMN-PT substrate in a 15 µm x 15 µm section with the inset highlighting a smaller ~7.2 µm x 7.2 µm sub-section. b) Illustration of local variation in surface roughness.

c. Negligible effect of Co layer oxidation

In order to characterize the films deposited (5 nm Ti + 11.5-12 nm Co), several material characterization techniques were performed.

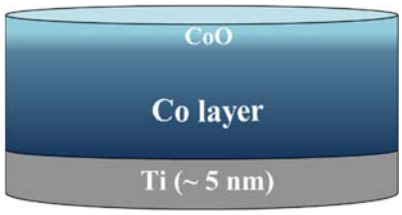

Figure S5. Elliptical Co nanomagnet with the native CoO layer (~1 nm). A 5 nm Ti layer is used to promote adhesion of the nanomagnet to the substrate.

- The Co layer (~11-12 nm) is *not* capped with any material and although this would lead to oxidation of the top 1-2 nanometers of the Co layer (Figure S5), if the experiment is conducted within 2-3 weeks, there will be no significant effect due oxidation on the ferromagnetic behavior of the bulk of the Co nanostructure.

- XPS studies of oxidation conducted on Co[12] showed ~1.7 nm of CoO forming after 10^3 hours. Since our experiments are performed within 10^3 hours, the resulting anti-ferromagnetic oxidation layer, CoO, would not be thick enough to have a detrimental effect on the magnetization of the metallic ferromagnetic Co layer in the elliptical nanomagnets.[13] Similar assumptions have also been made by Cui et al. on Ni films.[14]

d. Hysteresis (M-H) loops of thin-film Cobalt

In order to characterize the magnetic hysteresis of the cobalt used to fabricate our nanomagnets,

M-H plots (Figure S6) of a thin, 12 nm Co film were generated using a Quantum Design Versalab™ Vibrating Sample Magnetometer (VSM) at room temperature.

a)

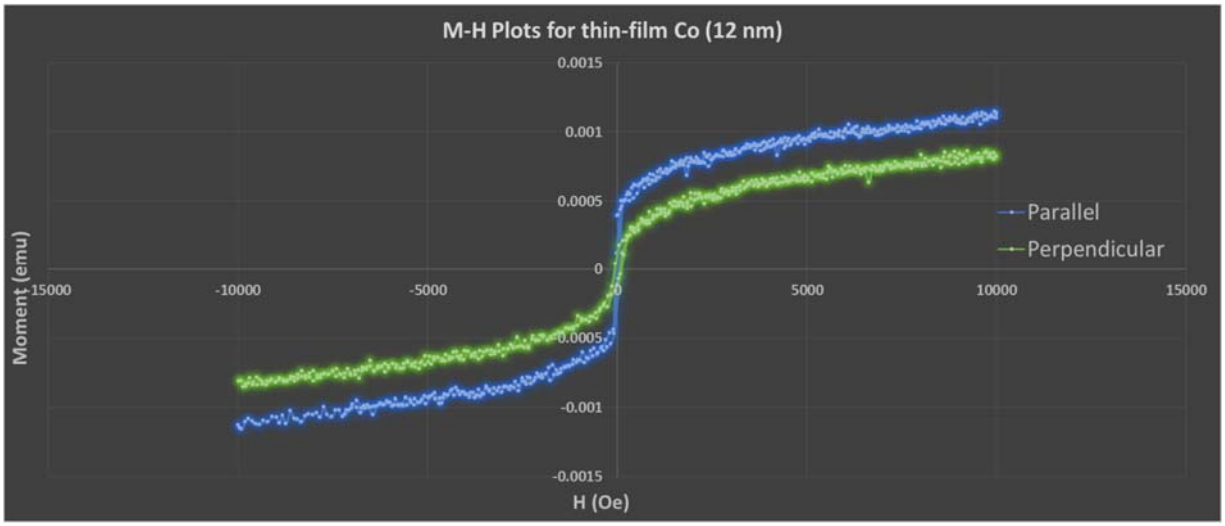

b)

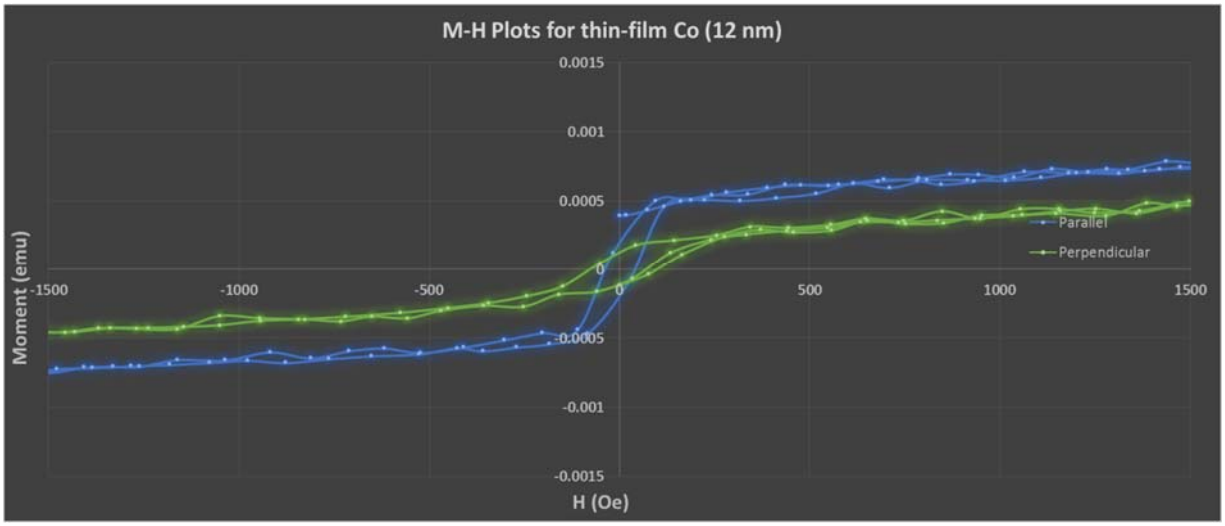

Figure S6. Hysteresis plots for 12 nm Co film. a) -10,000 Oe to +10,000 Oe. b) -1,500 Oe to +1,500 Oe

The effective sample size was ~2 mm x 3 mm. Figure S6a illustrates the M-H loops of the thin-film cobalt when subjected to a magnetic field from -10,000 Oe to +10,000 Oe. Two scenarios are plotted: i) H-field applied along the surface of the substrate (parallel, blue curve), and ii) H-field applied perpendicular to the face of the substrate (perpendicular, green curve). It can be seen that it is easier to magnetize the cobalt parallel to the surface than perpendicular to it. Thus, the "easy" axis of the magnetization is in-plane, or along the surface of the sample. The sample does not have perpendicular magnetic anisotropy (PMA).

Supplementary Section C: Magnetization Switching Results

a. Magnetic Force Microscopy (MFM) – Cycle 2 (Cycle 1 performed in main paper)

In the main paper, we present various magnetic force microscopy (MFM) images that illustrate magnetization switching in cases where the stress anisotropy energy of certain nanomagnets is greater than their shape anisotropy energy. Several scenarios are studied: a) nanomagnets with negligible dipole interaction (Case I), b) two dipole-coupled magnets (Case II), and c) array of three dipole-coupled magnets (Case III). These results represent the magnetic states before application of stress (nanomagnets are "initialized" to have their magnetizations point in the 'down' direction (↓) via a strong magnetic field) and after applying one cycle of stress ~80 MPa (Cycle 1). In order to test the repeatability of the magnetization switching demonstrated in the main paper, we perform another MFM study (Cycle 2) on the *same nanomagnet arrays* in which we re-"initialize" the magnetization, in this instance to (↑) with a strong magnetic field of ~200 mT directed along that direction. It is this Cycle-2 data that is presented in this section. After removing the field, we record the magnetic state at zero stress, then apply a strain of ~400 ppm that would produce a stress of ~80 MPa and capture the final magnetization orientation. In the following MFM images, we compare the pre- and post-stress magnetic states of nanomagnets in the three scenarios in Cycle 2.

Another issue that we must confirm – which did not occur in these experiments – is MFM tip-induced magnetization reorientation in the Co magnets. We perform several consecutive scans of the same nanomagnet array (top-down scan followed by bottom-up scan, and so on). Since no

switching occurs owing to scanning, we conclude that the magnetization of the MFM tip is not strong enough to affect the magnetization of the nanomagnets.

Note that the same nanomagnet arrays are investigated in both Cycle 1 and Cycle 2 for all three scenarios. Also, a small amount of nanomagnet sets appear to have contaminants on the surface after Cycle 2, possibly from contaminant accumulation on the MFM tips or from repeated applications of silver paste along the substrate edges. The nanomagnets affected by these contaminants are not considered in our conclusions about magnetization switching.

C.a.1: Isolated nanomagnets

In Figure S7, we show MFM images of isolated nanomagnets with negligible dipole interaction (~800 nm inter-magnet separation). Nanomagnets with lower shape anisotropy (nominally 200×175×12 nm^3) are shown in Figure S7 and we do observe magnetization rotation from (↑) to (↓) (yellow arrows), although these are not the same nanomagnets that switched in Cycle 1 (green arrows). This can be attributed to the fact that the stress induces a magnetization rotation (to the hard axis) in these nanomagnets, but once the stress is removed, there is a 50% probability of the magnetization rotating in either direction since they are under no (or negligible) dipole influence. Thus, a magnet that switched the first time need not switch the second time and vice-versa.

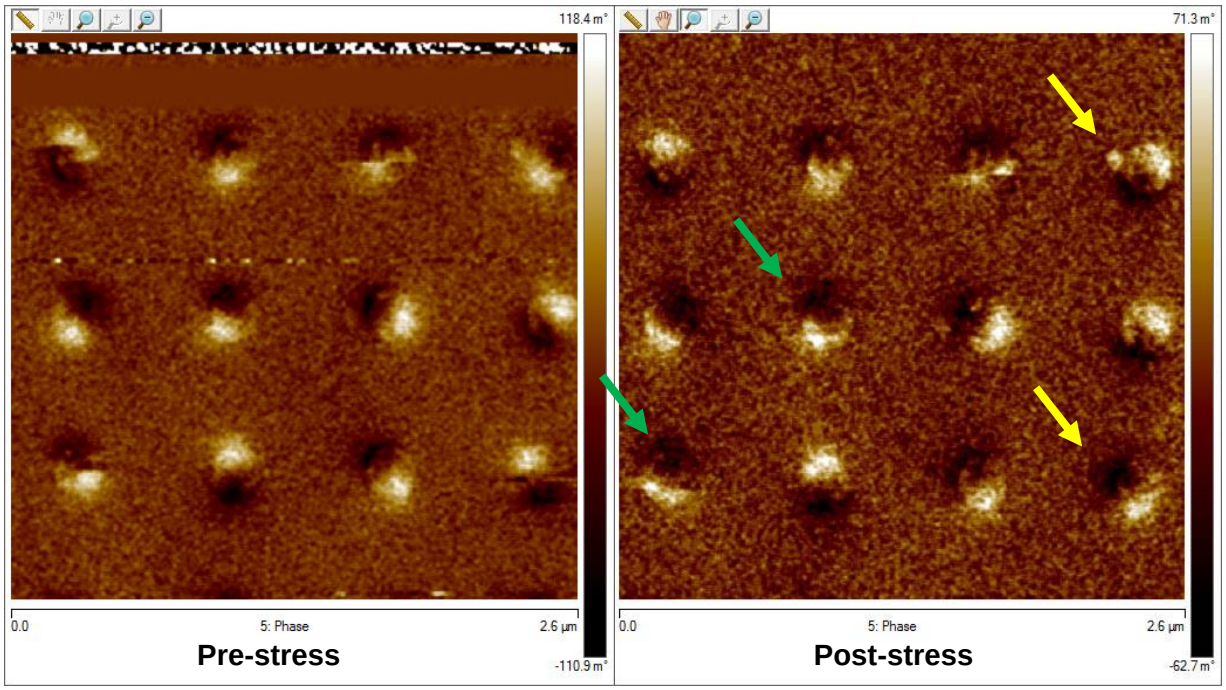

Figure S7: MFM phase images of Co nanomagnets with intermediate shape anisotropy (~200×175×12 nm^3) on bulk PMN-PT substrate with negligible dipole interaction with neighbors, in pre- and post-stress states. The nanomagnets are "initialized" to (↑) with a magnetic field of ~200 mT. When a stress of ~80 MPa is applied, magnetization rotation of ~90° takes place in those nanomagnets in which the stress anisotropy energy exceeds the shape anisotropy energy. When the stress is withdrawn, the magnetizations of these nanomagnets have a 50% probability of flipping from (↑) to (↓), with the yellow arrows highlighting such a scenario. The green arrows point to the nanomagnets that flipped their magnetization in Cycle 1, but not in Cycle 2.

C.a.2: Dipole-coupled pair

We also investigated dipole-coupled nanomagnets consisting of a highly shape-anisotropic "input" nanomagnet (~250×150×12 nm; left) that does not rotate significantly under stress and a less shape-anisotropic "output" nanomagnet (~200×175×12 nm; right) whose magnetization does rotate when stressed. It can be seen that two pairs of dipole-coupled nanomagnets (identified with yellow arrows) rotate from the initial (↑↑) state to the final (↑↓) state, indicating a flip in the output magnetization state upon application of stress (Figure S8a). Interestingly, the nanomagnet pair identified by the green arrow also exhibited magnetization switching in Cycle 1 (in which the rotation was from its pre-stress state of (↓↓) to a post-stress state of (↓↑)). Also, in order to ensure that the MFM tip does not induce magnetization rotation in the nanomagnets, we perform three consecutive scans (top-down, followed by bottom-up scans, and finally another top-down scan) of the same array shown in Figure S8a. Since all three scans are identical (Figure S8b), we can conclude that the MFM tip has a negligible effect on switching the magnetization of the nanomagnets.

a)

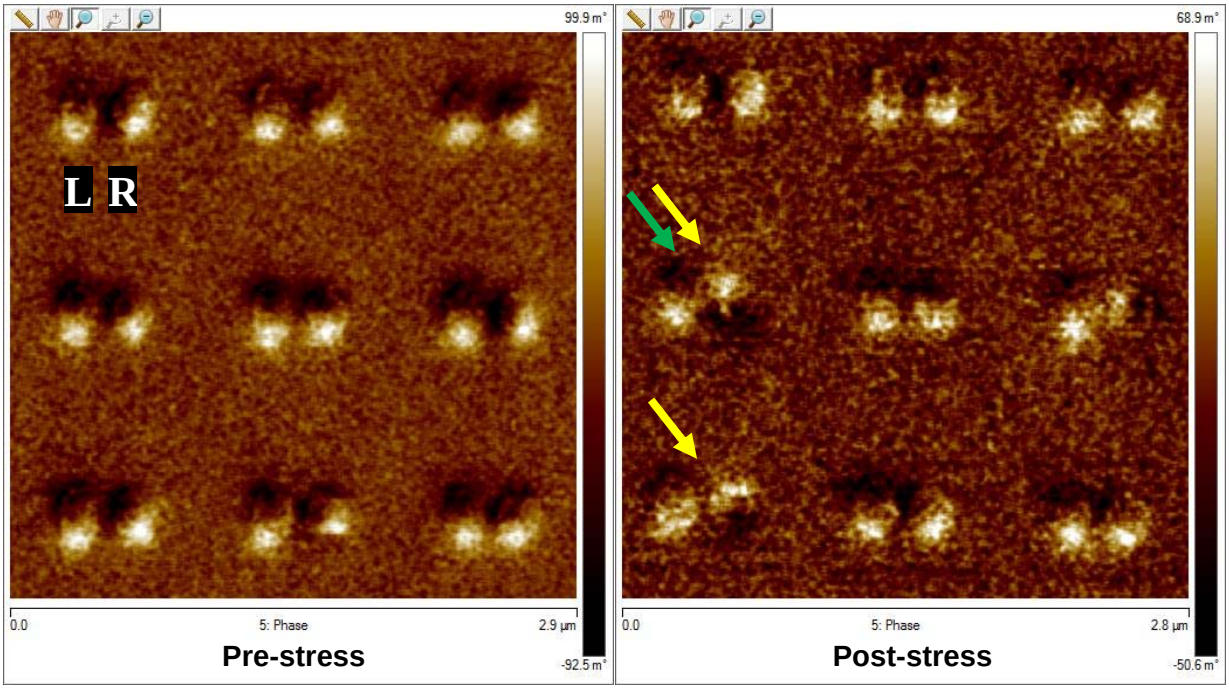
L R
0.0
5: Phase
2.9 µm
Pre-stress
0.0
5: Phase
2.8 µm
Post-stress

b)

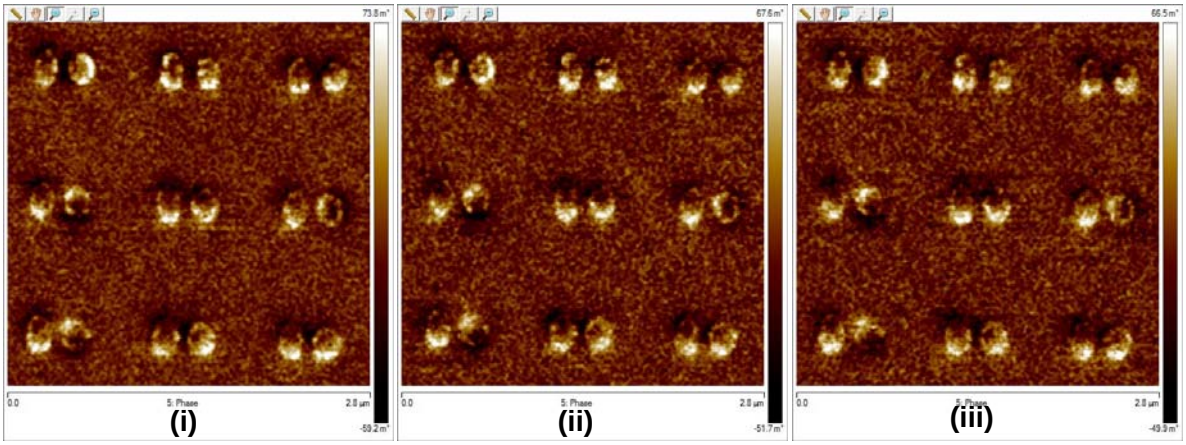
(i)
(ii)
(iii)

Figure S8: MFM phase images of dipole-coupled Co nanomagnets on bulk PMN-PT substrate with dipole interaction between neighbors in pre- and post-stress states. a, Nanomagnet pairs (**L**~250×150×12 nm^3, **R**~200×175×12 nm^3) with separation of ~300 nm between their centers. The initial state of the pairs is (↑↑) enforced with a magnetic field. Upon stress application of ~80 MPa, the magnetization of the "output" magnet **R** rotates by ~90° since the stress anisotropy energy is greater than its shape anisotropy energy barrier, while that of "input" **L** undergoes no significant rotation owing to the high shape anisotropy. When the stress is withdrawn, the magnetization of **R** rotates to the (↓) direction as dictated by its dipole interaction with **L**. This scenario is highlighted by the yellow arrows. Other nanomagnet pairs do not undergo this desired switching behavior, possibly due to variations in the fabrication process. The green arrow shows the nanomagnet pair that underwent magnetization switching in Cycle 1 as well [from (↓↓) to (↓↑)]. **b,** Consecutive MFM scans [(i) top-down, (ii) down-top, (iii) top-down] of the nanomagnet array of Fig. S8a. The identical states in all three cases confirm little or no tip-induced magnetization reorientation.

C.a.3: Dipole-coupled chain of nanomagnets

In Figure S9, we examine an array of three dipole-coupled nanomagnets of decreasing shape anisotropy and having nominal dimensions of 250×150×12 nm^3 (left), 200×175×12 nm^3 (center) and 200×185×12 nm^3 (right) with an inter-magnet separation of ~300 nm. As before, a global magnetic field (~200 mT) is applied to the nanomagnet arrays to "initialize" the nanomagnets to (↑↑↑). However, lack of precise lithographic control caused some nanomagnet dimensions to differ from the nominal dimensions. As a result, certain nanomagnets may have nearly circular shape with shape anisotropy energies that are lower than the dipole interaction energy due to their neighbors. In these cases, magnetization switching occurs as soon as the initializing magnetic field is removed, and before any stress is applied, because the dipole interaction between neighbors can overcome the small shape anisotropy energy barrier of the nearly-circular magnet and flip its magnetization without the aid of stress (no clocking required). This situation is identified by the red arrows in Figure S9, which show trios with initial pre-stress states of

(↑↓↑) instead of (↑↑↑). The yellow arrow in Figure S9a identifies a trio in which stress induces a magnetization rotation from its initial state (↑↑↑) to the desired final state (↑↓↑). In another magnet trio (blue arrow), the initial magnetization state is (↑↑↓). However, after applying the stress, the final state of the array is the desired state (↑↓↑). This signifies that when stress was applied, the magnetization of both the central and the right magnets get reoriented to the correct state based on dipole interactions with the "input" magnet on the left having the highest shape anisotropy (thereby, being marginally affected by stress). In another trio, with similar shape anisotropy variation in the nanomagnets (Figure S9b), we see correct magnetization switching from (↑↑↑) to (↑↓↑) after application of stress (yellow arrow) and from (↑↓↓) to (↑↓↑) (blue arrow). However, we also see instances of seemingly incorrect switching from (↑↑↑) to (↑↑↓) (white arrow). This may be due to several factors such as lithographic variances that result in the central nanomagnet having higher shape anisotropy than desired, stress variation in the substrate, etc. The green arrows identify nanomagnet arrays that switched in Cycle 1, with the dotted white box highlighting the set of arrays investigated in the main paper. It can be seen that neither of the three nanomagnet trios (green arrows) switched in Cycle 2. This can be attributed to the fact that the initial pre-stress state was probably incorrect and not the desired (↑↑↑) state.

a)

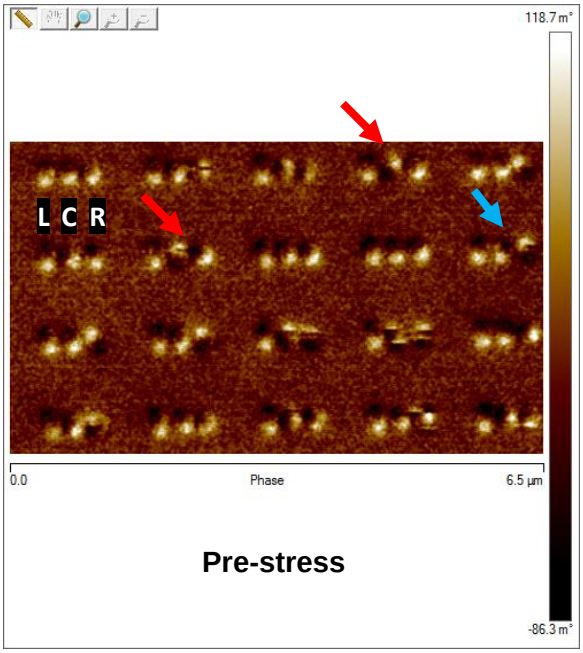
118.7 m°
L C R
0.0
Phase
6.5 µm
-86.3 m°
Pre-stress

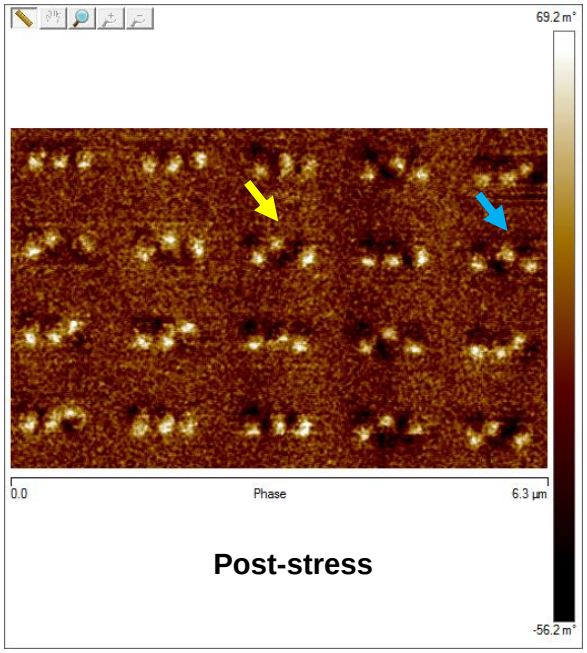
69.2 m°
0.0
Phase
6.3 µm
-56.2 m°
Post-stress

b)

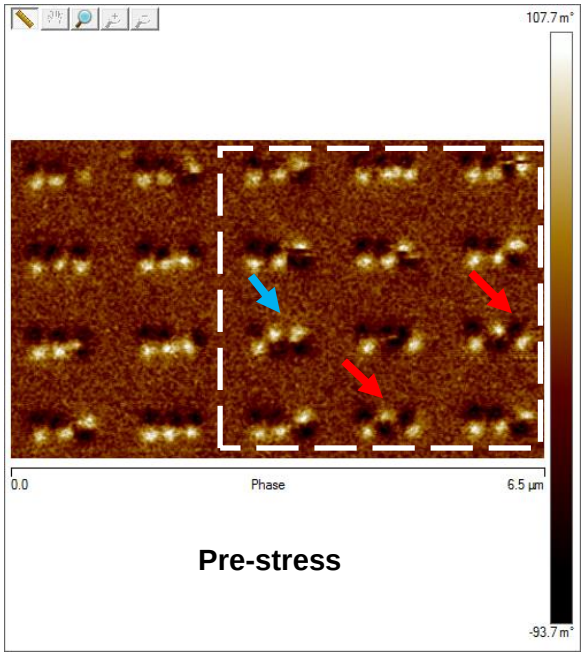
107.7 m°
0.0
Phase
6.5 µm
-93.7 m°
Pre-stress

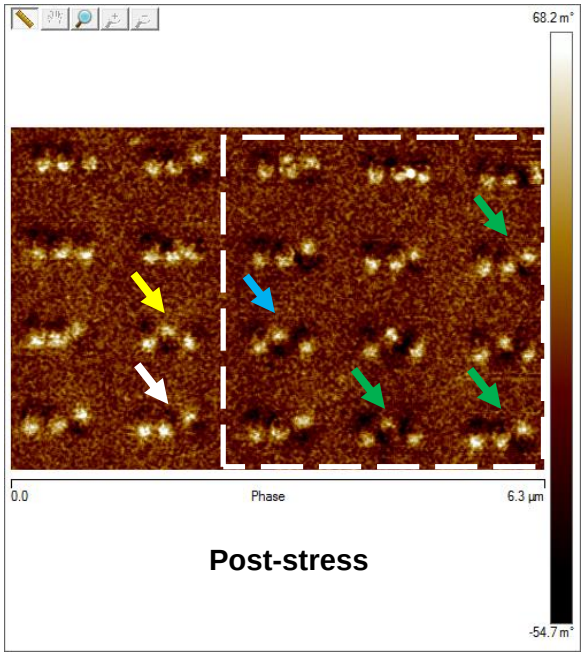
68.2 m°
0.0
Phase
6.3 µm
-54.7 m°
Post-stress

Figure S9: Dipole-coupled nanomagnet array consisting of three nanomagnets of decreasing shape anisotropy. (**a, b),** Nanomagnets (**L**, **C**, **R**) with nominal dimensions ~ 250×150×12 nm^3, 200×175×12 nm^3, 200×185×12 nm^3, respectively. The nanomagnet arrays are "initialized" to (↑↑↑) with a magnetic field. However, certain arrays have incorrect pre-stress initial states (red arrows), possibly due to lack of lithographic control that result in nanomagnets having shape anisotropy energies that are less than the dipole interaction energies they experience. That causes magnetization switching as soon as the initializing magnetic field is removed, and before any stress can be applied. The yellow arrow pinpoints arrays undergoing correct magnetization switching from (↑↑↑) to (↑↓↑). The blue arrow points to an array with incorrect initial states that settle to the desired final state of (↑↓↑) after application of stress ~80 MPa. The white arrow points to another array having a correct initial state but an incorrect final state of (↑↑↓) after applying stress. The green arrows identify nanomagnet arrays that switched in Cycle 1, with the dotted white box highlighting the set of arrays investigated in the main paper.

b. Switching "statistics" on other samples

While the above MFM and magnetization switching studies (Cycle 1 in the main paper, Cycle 2 in the previous section) were performed on the same sample, other such nanomagnets were fabricated on multiple other PMN-PT substrates and investigated.

It must be noted that while all the fabricated samples consist of multiple nanomagnets in multiple arrays, the focus of our studies is on demonstrating magnetization reversal due to strain in a particular nanomagnet (or nanomagnet pairs for dipole-coupled NOT logic and information propagation in three nanomagnet arrays) in a deterministic and repeatable manner.

In a particular array of 9 nanomagnets (as illustrated in our results), in which we expect magnetization rotation due to stress, the 'nominal' dimensions are chosen so that the shape anisotropy is *less than* the stress anisotropy. However, post-lithography and lift-off, there is a slight deviation from the 'nominal' dimensions. Therefore, out of the 9 nanomagnets, there is a fraction in which the shape anisotropy becomes *greater than* the stress anisotropy. We deem this an issue of fabrication-related limitation, rather than a fundamental issue with regard to the physics of the switching behavior. The SEM images of Figure S10 show examples of the variation in lateral dimensions of the fabricated Co nanomagnets on a PMN-PT substrate. It is clear that many nanomagnets would have huge shape anisotropy due to fabrication imperfection (deviation from nominal dimensions) that prevents them from switching.

Consequently, the 'yield' of observable magnetization switching in these fabricated nanomagnets is not the main focus of our studies. The primary goal is to investigate switching recurrence (through multiple stress cycles) in those nanomagnets that *do* show magnetization rotation. The fact that high error rates and fabrication tolerances affect the yield of switching does not detract

from the underlying physics driving this scheme. This is also shown in the observation that switching events (albeit low in number) occur in every sample tested.

The important aspect, therefore, is how often the switching takes place in a particular nanomagnet (or dipole coupled pair) once we have identified the nanomagnet(s) whose shape anisotropy is less than the stress anisotropy and, therefore, are expected to switch consistently.

Multiple cycles of "initialization" (with a magnetic field) and electric field/stress application were scheduled in order to study important aspects of the magnetization switching, such as repeatability, switching statistics, randomness of switching, etc. However, due to the frailty of the PMN-PT substrate, especially when subjected to repeated cycles of high electric fields, there is inevitable crack formation in the substrate which ultimately causes sample failure. As a result, substrate degradation used to occur after 2-3 cycles of stress application (due to the large electric fields applied to the substrate).

One particular method of poling the PMN-PT substrates, involving elevated temperature of the oil bath in which we immerse the PMN-PT during poling[15], minimized the amount of post-poling cracks within the substrate by reducing the large strain variation of ferroelastic domain switching. While this seems to prevent crack formation after poling, it does not prevent eventual substrate degradation after several cycles of electric field application (2-3 stress cycles). This prevents the compilation of an extensive set of switching statistics.

a)

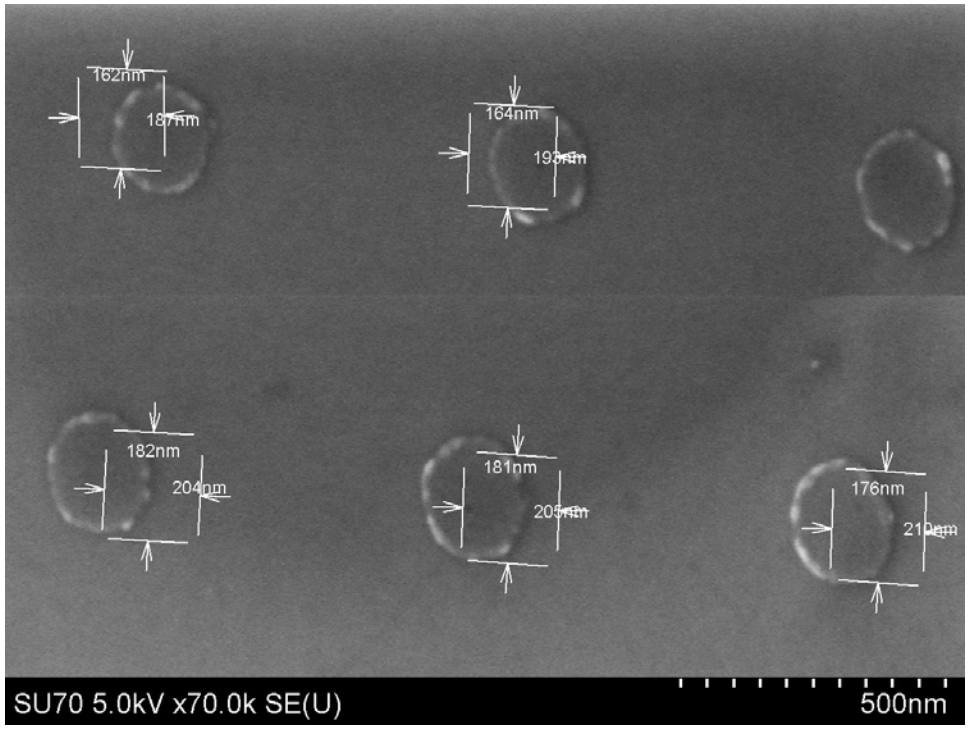

b)

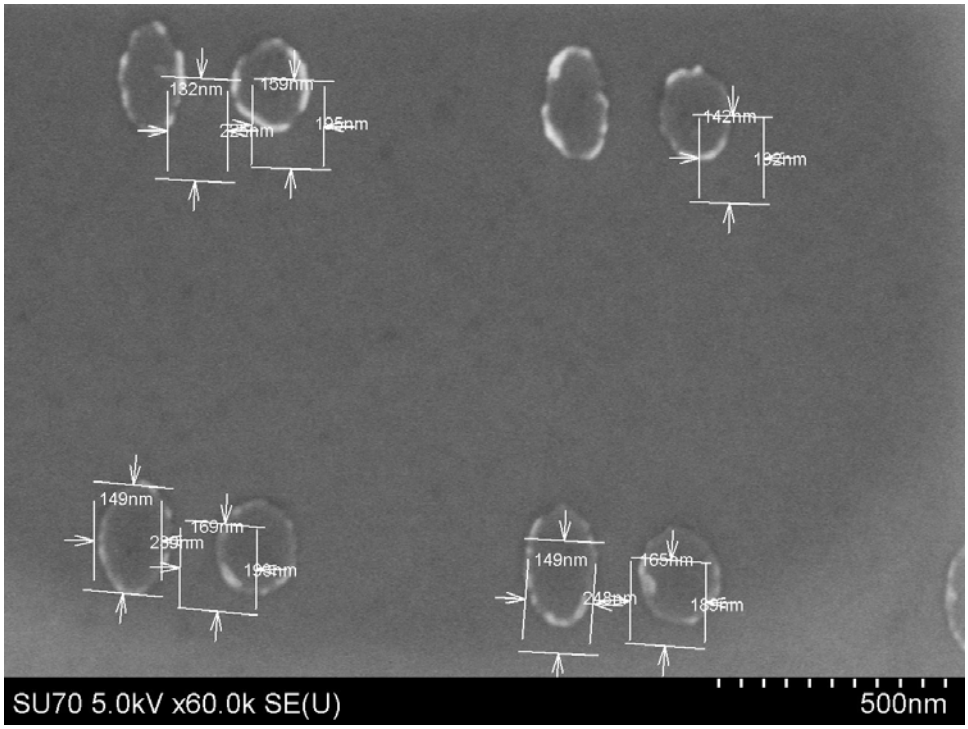

Figure S10. SEM images of a) isolated nanomagnet with nominal dimensions of (200 nm × 185 nm × 12 nm), and b) dipole-coupled nanomagnets with nominal dimensions of (250 nm × 150 nm × 12 nm, 200 nm × 175 nm × 12 nm), showing fabrication variation in lateral dimensions. Note: A slight drift in the electron beam during scanning resulted in a shift in the measurement markers.

Hence, the best "confirmative statistics" that we could obtain was 2 out of 2 switching events. Multiple samples were fabricated and comprehensively analyzed for switching behavior. Each of these 5 samples shows switching events, although the yield of nanomagnets that switch is consistently low.

Further, if we focus on a specific nanomagnet (isolated), or pair (dipole coupled NOT gate), or array of three (dipole coupled Bennett clocking) in these samples, we find the switching events to be as follows:

Table S3. Switching events (best) in Co nanomagnets on PMN-PT substrate after stress application

Nanomagnet dimensions	**# of switching events/# of stress cycles (best results only across 5 different samples)**
Isolated (high shape anisotropy) 250×150×12 nm^3	0 out of 3 *(This particular nanomagnet is deliberately designed NOT to switch)*
Isolated (medium shape anisotropy) 200×175×12 nm^3	1 out of 2 *(expect isolated magnets to only switch 50% of the time, as once stress is withdrawn, it could relax from the hard axis to either easy direction)*
Isolated (low shape anisotropy) 200×185×12 nm^3	1 out of 2 OR 2 out of 3 OR 1 out of 3 *(For 3 cycles it cannot switch "1.5 times", it would switch 1 on 3 or 2 on 3 times)*
Dipole-coupled NOT gate (250×150×12 nm^3, 200×175×12 nm^3)	2 out of 2 *(only 2 cycles before substrate failure)*
Array of 3 magnets (Bennett clocking) (250×150×12 nm^3, 200×175×12 nm^3, 200×185×12 nm^3)	1 out of 2 *(for 3 magnets, where 2 magnets can switch, the chance of getting "up", "down", "up" is 1 out of 4 or 25%. So, the fact this works 50% of the time shows dipole coupling affects the switching)*

Table S3 highlights the best switching "statistics" that we encountered over *two-three* stress cycles across the 5 different PMN-PT substrates, for a particular nanomagnet (isolated, pair or array).

The Dipole-coupling effect

Consider Figure 3 of the main paper involving a chain of three nanomagnets. If dipole coupling played no role, then the second ("C") and third ("R") nanomagnet in each chain that switch in response to the state of the first highly anisotropic nanomagnet ("L'), can assume 2^2 =4 possible orientations. Thus, the states seen should be:

1. "↓↑↑"
2. "↓↑↓"
3. "↓↓↑"
4. "↓↓↓"

However, in the panel of nanomagnets shown, either these nanomagnets don't switch at all or are ambiguous (lithography issues) or switch unambiguously to PREDOMINANTLY the "↓↑↓" state. If dipole coupling played no role, we should see "1", "2", "3" and "4" with equal probability. But we see 3 clear instances of "↓↑↓", and NO instance of "↓↑↑" and just one instance of "↓↓↑" (explained by second nanomagnet's magnetization was pinned, so only the 3rd responded). We do see "↓↓↓" but that can be accounted for by no switching occurring at all due to lithography issues!

Clearly, this provides additional evidence of the effect of dipole coupling on a NOT gate and logic propagation.

Low Yield Explanation

The low 'yield' of switching events in a set of fabricated nanomagnetic elements (isolated, pair or array) is one of the challenges of nanomagnetic logic (NML), where high switching error rates accruing from imperfect fabrication are frequently encountered. In recent work studying error rates in NML circuits with magnetic field-based switching[16], error rates as high as 77% were observed for low aspect ratio nanomagnetic elements and 76% for high aspect ratio elements in chains of nanomagnets. This was attributed to fabrication process-related variations, rough edges, etc. Only with careful fabrication methods (double e-beam exposure technique) that reduced the inter-magnet spacing, the error rates were brought down to 41% and 30% respectively, which are of course still very high.

Switching "Statistics" Explanation

Another important consideration when studying magnetization reversal due to stress in these magnetostrictive nanomagnets is that the effective magnetic field may just be able beat the shape anisotropy barrier but the switching can still be impeded by other effects such as pinning sites, defects, etc. The reason for the switching inconsistency in the nanomagnets (from stress cycle to stress cycle) can be explained as follows:

The stress anisotropy energy of a nanomagnet can be expressed as:

$$E_{stress-anisotropy} = \mu_0 M_s H_{eff} \sim \left(-\tfrac{3}{2}\lambda_s\right)\sigma$$

or, $$H_{eff} \sim \frac{1}{\mu_0 M_s}\left(-\tfrac{3}{2}\lambda_s\right)\sigma$$

where H_{eff} is the effective magnetic field, μ_0 is the permeability of free space ($4\pi \cdot 10^{-7}$ H·m^{-1}), M_s is the saturation magnetization of Cobalt (14.22×10^5 A·m^{-1}), ($^3/_2 \lambda_s$) is the saturation magnetostriction of Co (50 ppm) and σ is the stress applied to the nanomagnet (~ 80 MPa).
All this yields a value of H_{eff} ~ 30 Oe. While the nanomagnet's size and shape (low aspect ratio) are designed so that this "effective field due to stress" can beat the shape anisotropy barrier, the effective field (driving force) may not be sufficient to overcome the effects of pinning sites, edge roughness, etc., when considering the effects jagged edges, pinning sites, etc.

In fact, the M-H curve of Co film shows that the $H_{coercivity}$ is ~50 Oe (see the VSM data of the magnetization curves of films) but this is due to both substrate clamping and pinning sites. The $H_{coercivity}$ could be smaller in the nanostructures as the strain from the bulk substrate is transferred to the nanomagnet to switch it, so the substrate does not cause a "clamping effect". Hence, the coercivity in the magnets may be comparable to or smaller than H_{eff} due to strain. As a result, some nanomagnets switch, but the "switching statistics" (fraction of successful switching events, even with maximum stress applied) is considerably low.

All this points to a fundamental limitation of strain clocking with Co nanomagnets. Clearly, if materials with better magnetoelastic coupling and higher magnetostriction could be fabricated (e.g. Terfenol-D, with 30 time higher magnetostriction), then the switching probability could improve significantly. This is because H_{eff} due to strain ~ 1000 Oe for such materials stressed by ~80 MPa and can easily overcome any pinning sites and other defects that lead to high coercivity. Thus, the low yield of switching events in a large nanomagnet array could be

attributed to the weak magnetoelastic coupling (material properties) of the magnetostrictive material investigated (Cobalt).

This process and materials-related issue, although highly important for technological applications, does not circumscribe the physics involved in strain-based magnetization switching. This has happened before, in other fields as well. Spin Hall effect was well known earlier, but only recent discovery of large Spin-Hall angles in heavy metals (Pt, W and Ta) allowed efficient magnetization reversal using Spin-Hall effect.[17–19]

Supplementary Section D: Global vs. Local clocking and energy dissipation calculation

In the main paper, strain-induced magnetization switching in elliptical nanomagnets was accomplished using a *global* stress on a bulk PMN-PT substrate. A Boolean NOT logic gate was also demonstrated, along with unidirectional bit information propagation. An alternate scheme involves applying *local* stress in a phased manner to clock nanomagnets of nominally identical dimensions unidirectionally in the manner of Ref. 14 as shown in Figure S11.

Each electrode pair is activated by applying an electrostatic potential between both members of that pair and the grounded substrate. Since the electrode in-plane dimensions are comparable to the piezoelectric film thickness, the out-of-plane (d_{33}) expansion/contraction and the in-plane (d_{31}) contraction/expansion of the piezoelectric regions underneath the electrodes produce a highly localized strain field under the electrodes[14]. Furthermore, since the electrodes are separated by a distance 1–2 times the piezoelectric film thickness, the interaction between the local strain fields below the electrodes will lead to a biaxial strain in the piezoelectric layer underneath the magnet[14]. This biaxial strain (compression/tension along the line joining the electrodes and tension/compression along the perpendicular axis) is transferred to the magnet, thus rotating its magnetization. This happens despite any substrate clamping and despite the fact that the electric field in the PZT layer just below the magnet is approximately zero since the metallic magnet shorts out the field[14]. The electrode pairs are activated sequentially in the manner shown in Figure S11 to implement both NOT function and for unidirectional propagation of information along a chain of nanomagnets.

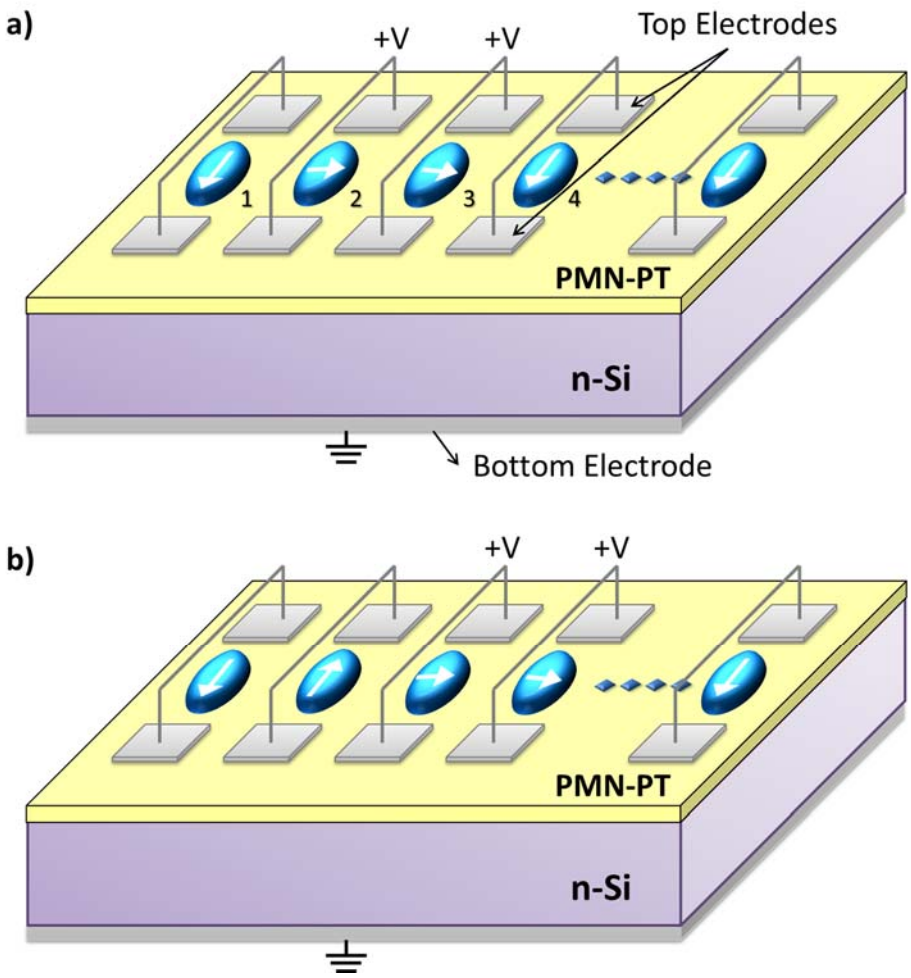

Figure S11: Local clocking of nanomagnets using the Bennett clocking scheme. Ideally, if a local strain-clocking scheme is employed, stress can be applied *selectively* to targeted nanomagnets via individual electrodes[14]. Here all magnets are assumed to be nominally identical. (*a*) To propagate the magnetization state of the input magnet **1**, a voltage (+V) is applied to nanomagnets **2** and **3** simultaneously to generate a stress σ to 'clock' them. (*b*) In the next phase of the clock cycle, the voltage (stress) is removed from **2**, while **3** and **4** are now clocked, resulting in the magnetization of **2** rotating and settling to the desired 'up' direction. This clock cycle is applied to successive nanomagnet pairs along the array with the input data propagating unidirectionally and replicated in every odd-numbered nanomagnet.

To highlight the potential energy efficiency of strain clocked nanomagnetic logic, we calculate the energy dissipation per clock cycle for the local clocking scheme. To generate a strain of ~400 ppm, a conservative estimate of the electric field needed for a PMN-PT film with d_{33} = ~(1500-

2500) pm/V [5] and d_{31} = ~ -(700-1300) pm/V [5] in the above configuration is ~400 kV/m. To apply this field locally between the electrode and the substrate for a PMN-PT film of thickness t~200 nm, the voltage required would have been ~80 mV. The capacitance between the electrode pair and substrate is calculated by treating them as two flat plate capacitors in parallel. The area of each plate is A = 4×10^{-14} m^2 (assume square electrode of width ~200 nm). The total capacitance including both electrodes is, C = 2 $\varepsilon_0\varepsilon_r A/t$ is ~10 fF. Assuming all the energy involved in charging the capacitor to strain the nanomagnet is lost, the energy dissipation/clock cycle, $E_d = 1/2\ CV^2$ = 32×10^{-18} J (32 aJ). Scaling the nanomagnet dimensions to ~100 nm and the square electrode width to ~100 nm will allow one to reduce the PMN-PT thickness to ~100 nm. This will reduce the switching voltage required to ~40 mV and the total capacitance to ~5 fF, making the energy dissipation go down to ~4 aJ. Moreover, if highly magnetostrictive materials such as Terfenol-D can be used instead of cobalt, the voltage needed can be decreased to ~8 mV and the energy dissipated in the switching circuit to ~0.16 aJ. Additional dissipation in the magnet due to Gilbert damping must then be taken into account and would roughly be ~1 aJ per clock cycle for a 1 GHz clock.[20] Therefore, the total dissipation in switching could be as low as ~1 aJ per clock cycle which is two to three orders of magnitude lower than what current transistors dissipate during switching[21] and one order of magnitude lower than the calculated dissipation in switching magnets with spin Hall effect.[19] That would make this scheme the most energy-efficient clocking mechanism extant.

References

(1) Davis, J. Introduction to Cobalt and Cobalt Alloys. In *Nickel, cobalt, and their alloys*; ASM International: Materials Park OH, 2000; p. 345.

(2) Bozorth, R. M. *Ferromagnetism*; Wiley, 1993.

(3) Long, J. *Iron Cobalt Boride and Iron Zirconium Silicide-Based Nanocomposite Soft Magnetic Alloys and Application*; 2008.

(4) Viehland, D.; Li, J.-F. Young's Modulus and Hysteretic Losses of 0.7Pb(Mg[sub 1/3]Nb[sub 2/3])O[sub 3]–0.3PbTiO[sub 3]: Single versus Polycrystalline Forms. *J. Appl. Phys.* **2003**, *94*, 7719.

(5) Luo, L.; Zhao, X.; Luo, H. Single Crystal PZN-PT, PMN-PT, PSN-PT and PIN-PT-Based Piezoelectric Materials. In *Advanced Piezoelectric Materials: Science and Technology*; Uchino, K., Ed.; Woodhead Publishing, 2010; p. 696.

(6) Xia, Z.; Wang, L.; Yan, W.; Li, Q.; Zhang, Y. Comparative Investigation of Structure and Dielectric Properties of Pb(Mg1/3Nb2/3)O3–PbTiO3 (65/35) and 10% PbZrO3-Doped Pb(Mg1/3Nb2/3)O3–PbTiO3 (65/35) Ceramics Prepared by a Modified Precursor Method. *Mater. Res. Bull.* **2007**, *42*, 1715–1722.

(7) Kelly, J.; Leonard, M. Effect of Composition on the Electromechanical Properties of (1-X) Pb (Mg1/3Nb2/3) O3− XPbTiO3 Ceramics. *J. Am. Ceram. Soc.* **1997**, *80*, 957–964.

(8) Chen, K.-P.; Zhang, X.-W.; Luo, H.-S. Electric-Field-Induced Phase Transition in <001>-Oriented Pb(Mg 1/3 Nb 2/3)O3 -PbTiO 3 Single Crystals. *J. Phys. Condens. Matter* **2002**, *14*, L571–L576.

(9) Cullity, B. D.; Graham, C. D. *Introduction to Magnetic Materials*; Wiley, 2009.

(10) Osborn, J. J. Demagnetizing Factors of the General Ellipsoid. *Phys. Rev.* **1945**, *67*, 351–357.

(11) Peirce, B. *A Short Table of Integrals*; 4th ed.; Ginn and Company: Boston, 1957.

(12) Gan, L.; Gomez, R. D.; Powell, C. J.; McMichael, R. D.; Chen, P. J.; Egelhoff, W. F. Thin Al, Au, Cu, Ni, Fe, and Ta Films as Oxidation Barriers for Co in Air. *J. Appl. Phys.* **2003**, *93*, 8731.

(13) Welp, U.; te Velthuis, S. G. E.; Felcher, G. P.; Gredig, T.; Dahlberg, E. D. Domain Formation in Exchange Biased Co/CoO Bilayers. *J. Appl. Phys.* **2003**, *93*, 7726.

(14) Cui, J.; Hockel, J. L.; Nordeen, P. K.; Pisani, D. M.; Liang, C.; Carman, G. P.; Lynch, C. S. A Method to Control Magnetism in Individual Strain-Mediated Magnetoelectric Islands. *Appl. Phys. Lett.* **2013**, *103*, 232905.

(15) Li, F.; Wang, L.; Jin, L.; Xu, Z.; Zhang, S. Achieving Single Domain Relaxor-PT Crystals by High Temperature Poling. *CrystEngComm* **2014**, *16*, 2892.

(16) Shah, F. A.; Csaba, G.; Niemier, M. T.; Hu, X. S.; Porod, W.; Bernstein, G. H. Error Analysis for Ultra Dense Nanomagnet Logic Circuits. *J. Appl. Phys.* **2015**, *117*, 17A906.

(17) Miron, I. M.; Garello, K.; Gaudin, G.; Zermatten, P.-J.; Costache, M. V; Auffret, S.; Bandiera, S.; Rodmacq, B.; Schuhl, A.; Gambardella, P. Perpendicular Switching of a Single Ferromagnetic Layer Induced by in-Plane Current Injection. *Nature* **2011**, *476*, 189–193.

(18) Pai, C.-F.; Liu, L.; Li, Y.; Tseng, H. W.; Ralph, D. C.; Buhrman, R. A. Spin Transfer

Torque Devices Utilizing the Giant Spin Hall Effect of Tungsten. *Appl. Phys. Lett.* **2012**, *101*, 122404.

(19) Bhowmik, D.; You, L.; Salahuddin, S. Spin Hall Effect Clocking of Nanomagnetic Logic without a Magnetic Field. *Nat. Nanotechnol.* **2014**, *9*, 59–63.

(20) Salehi Fashami, M.; Roy, K.; Atulasimha, J.; Bandyopadhyay, S. Magnetization Dynamics, Bennett Clocking and Associated Energy Dissipation in Multiferroic Logic. *Nanotechnology* **2011**, *22*, 155201.

(21) International Technology Roadmap for Semiconductors www.itrs.com.